Influence of the Chemical Composition on Structural Properties and Electrical Conductivity of Y−Ce−ZrO_2

A. G. Belous,* K. V. Kravchyk, and E. V. Pashkova

V. I. Vernadskii Institute of General and Inorganic Chemistry, 32/34 Palladina Avenue, 03680, Kyiv 142, Ukraine

O. Bohnke and C. Galven

Laboratoire des Oxydes et Fluorures (UMR 6010 CNRS), Institut de Recherche en Ingénierie Moléculaire et Matériaux Fonctionnels (FR 2575 CNRS), Université du Maine Av O. Messiaen, 72085 Le Mans Cedex 9, France

Received February 2, 2007. Revised Manuscript Received May 14, 2007

The influence of the chemical composition on structural properties and electrical conductivity of solid solutions based on the system Y−Ce−ZrO_2 obtained by the hydroxide precipitation method is investigated. The samples are studied by combining impedance spectroscopy, X-ray powder diffraction, and scanning electron microscopy measurements so as to determine the effect of the phase composition on both the microstructure and the electrophysical properties of the ceramics. The oxygen partial pressures, at which p-type or n-type electronic conductivity appears predominantly, are determined for these ceramics in the temperature range from 920 to 1020 K. Therefore, the oxygen activity domain into which the ceramic samples are predominantly ionic conductors is found as a function of temperature for different chemical compositions of the Ce and Y substituted zirconium oxide.

Introduction

Y_2O_3 stabilized zirconium oxide (Y−ZrO_2) is widely used in various electrochemical devices (fuel cells, oxygen sensors, etc.).[1−3] The disadvantages of such materials, based on Y−ZrO_2, are a high sintering temperature ($T_s \geq 1870$ K) and a structural instability at high temperatures in a humid atmosphere.[4−6] The use of precursors made of nanosized particles can be of a great interest to decrease the sintering temperature, whereas the structural stability can be improved through the development of new complex stabilizers.

One of the effective ways to obtain nanosized particles of ZrO_2-based systems may be the hydroxide precipitation method, which is distinguished from other chemical "wet" methods by its simplicity and availability. This method, unlike the sol−gel method, allows additional removal of detrimental impurities and unwanted reaction products. However, the heat treatment of these precipitates, obtained by the coprecipitation method at high temperatures, often results in the formation of hard powders. These powders require then a milling for a long time, which has an adverse effect on the properties of the ceramics based on them. It should also be noted that nanoparticles are inclined to self-organization during synthesis.[7] In many cases, this allows nanosized fractally organized powders to be obtained, which are characterized by weak bonds between particles. Therefore, nanoscale ceramics based on them can be obtained at relatively low temperatures.

Increased stability of the structure of materials based on the system ZrO_2−Y_2O_3 can be achieved by addition of cerium oxide (5−20 mol %).[8] However, solid solutions based on ZrO_2−Y_2O_3−CeO_2 are characterized by smaller values of oxygen conductivity in comparison with the ZrO_2−Y_2O_3 system.[9] As was revealed in several investigations,[9−13] materials based on the system ZrO_2−Y_2O_3−CeO_2 can be ionic conductors[10] or electronic−ionic conductors[9,11−13] depending on composition, temperature, and method of synthesis used. Their oxygen ionic conductivity, which is sufficiently high especially in the low- and medium-temperature ranges, allows them to be used as oxygen sensors or λ-sensors for automobiles.[10] Furthermore, materials based on the system ZrO_2−Y_2O_3−CeO_2 are particularly attractive as advanced electrode materials for full cells because they have a good chemical and thermal compatibility with zirconium electrolyte.[9] However, the application of ZrO_2-based materials doped with cerium as solid electrolytes in

* Corresponding author. Tel.: +380-42-42-211. Fax.: +380-42-42-211. E-mail address: belous@mail.kar.net.

(1) Chiodelli, G.; Flor, G.; Scagliotti, M. *Solid State Ionics* **1996**, *91*, 109.
(2) Lee, J. H.; Kim, J.; Kim, S. W.; Lee, H. W.; Song, H. S. *Solid State Ionics* **2004**, *166*, 45.
(3) Kawamura, K.; Watanabe, K.; Hiramatsu, T.; Kaimai, A.; Nigara, Y.; Kawada, T.; Mizusaki. J. *Solid State Ionics* **2001**, *144*, 11.
(4) Sato, T; Shimada, M. *J. Am. Ceram. Soc.* **1985**, *68* (No. 6), 356.
(5) Sato, T.; Ohtaki, S.; Shimada, M. *J. Mater. Sci.* **1985**, *20*, 1466.
(6) Kuwabara, M.; Ashizura, M.; Kubota, Y.; Tsukidate, T. *J. Mater. Sci. Lett.* **1986**, *5*, 7.
(7) Kravchyk, K. V.; Gomza, Y. P.; Pashkova, E. V.; Belous, A. G.; Nesin, S. D. *Inorg. Mater.* **2007**, *43* (No. 3), 258.
(8) Duh, J. G.; Lee, M. Y. *J. Mater. Sci.* **1989**, *24*, 1959.
(9) Lee, C. H.; Choi, G. M. *Solid State Ionics* **2000**, *135*, 653.
(10) Karavayev, J. N.; Burmakin, Y. I. *Elektrokhimiya* **1992**, *28* (No. 10), 1484.
(11) Chun, C. M.; Mumford, J. D.; Patel, J.; Ramanarayanan, T. A. *J. Electroceramics* **2003**, *10*, 221.
(12) Chiou, B.; Dai, H.; Duh, J. *J. Am. Ceram. Soc.* **1990**, *73* (No. 4), 866.
(13) Arashi, H.; Naito, H.; Nakata, M. *Solid State Ionics* **1995**, *76*, 315.

10.1021/cm070319j CCC: $37.00
Published on Web 09/22/2007

electrochemical devices is limited due to the increase of the electronic conductivity with the increase of cerium content.[11−13] Therefore, it is important to maintain both a structural stability and a low electronic conductivity in a wide range of oxygen partial pressures and, at the same time, to increase the oxygen conductivity of the materials of the system $ZrO_2-Y_2O_3-CeO_2$ by changing the CeO_2/Y_2O_3 ratio.

The main purpose of the present paper is then to investigate the effect of the chemical composition on the electrophysical properties of the solid solutions $ZrO_2-Y_2O_3-CeO_2$ obtained by hydroxide precipitation from solutions.

Experimental Section

Ceramic samples of nominal compositions 0.93/0.06/0.01 $ZrO_2-CeO_2-Y_2O_3$ (I), 0.88/0.09/0.03 $ZrO_2-CeO_2-Y_2O_3$ (II), and 0.84/0.08/0.08 $ZrO_2-CeO_2-Y_2O_3$ (III) were investigated. The change of composition was performed according to the results of our preliminary investigations and also because one of our goals was to prepare oxygen conductors. Therefore, selection criteria were the absence of monoclinic (nonconducting) phase and the tendency to obtain a monophase material with high-conducting cubic structure of the type CaF_2. This can be achieved by simultaneously decreasing the oxide−stabilizers ratio (CeO_2/Y_2O_3) and increasing their total amount ($CeO_2 + Y_2O_3$). The results of our preliminary investigations showed that these above-mentioned compositions have a low sintering temperature (1670 K). Therefore, we synthesized hydroxide precursors of the $ZrO_2-Y_2O_3-CeO_2$ system by the two following methods: (i) a sequential precipitation of hydroxides (named hereafter SPH) and (ii) the coprecipitation of hydroxides (named hereafter CPH). A concentrated aqueous solution of ammonia was used for precipitation. Used as original reactants were 2 M water solutions of $ZrOCl_2$, $Y(NO_3)_3$, and $Ce(NO_3)_4$.

Powders of precursors were calcined at 1120 K for 2 h. To prepare molding powder, a solution of poly(vinyl alcohol) was used. Pellets were uniaxially pressed at $P = 200$ MPa. Samples were sintered at $T = 1670$ K for 2 h.

X-ray powder diffraction (XRPD) data were collected using a DRON 4-07 diffractometer (Cu Kα radiation; 40 kV, 18 mA), in the 2Θ range from 10 to 150°, in a step-scan mode with $\Delta 2\theta = 0.01$ and an exposure time of 10 s for each point. SiO_2 (standard 2Θ) and Al_2O_3 (certified standard of intensity) were used.[14] The grain size in the ceramic samples was determined by scanning electron microscopy using a Hitachi 2300 scanning electron microscope. The size distribution of the aggregated particles, after heat treatment at 870 K, was determined with a HELPS 348 Sympatec particle analyzer. Powders were analyzed after in situ ultrasonic vibration for 3 min.

The electrophysical properties of the samples were investigated by complex impedance spectroscopy and by the Hebb−Wagner polarization technique. To avoid any confusion in the remainder of this paper, we have to recall that the complex impedance spectroscopy is not able to determine the nature of the charged carriers (ions or electrons). Therefore, this technique allows the conductivity of the samples whatever the nature of the charged carriers to be determined. By this technique both the bulk conductivity and the total conductivity of the samples under study are determined (in this paper, the term "total conductivity" means bulk + grain boundary conductivity). On the other hand, the Hebb−Wagner polarization technique will allow the electronic conductivity alone to be determined.

(14) *Certificate of Analysis. Standard Reference Material 1976, Instrument Sensitivity Standard for X-ray Powder Diffraction*; National Institute of Standards & Technology: Gaithersburg, 1991.

Table 1. Structural Parameters of the SPH and CPH Samples Determined Using the Small-Angle X-ray Dispersion Data[a]

sample	T (K)	level of aggregation	type of fractal	s	D	R_g, nm	d_s, nm
SPH	295	1	M	−1.1	1.1	3.0	7.7
	295	2	S	−3.63	2.37	30	77.4
	295	3	M	−2.8	2.8	130	335
CPH	295	1	M	−1.5	1.5	2.5	6.5
	295	2	S	−3.4	2.6	22	56.8
	295	3	S	−3.3	2.7	150	387

[a] M is the mass fractal, and S is the surface fractal; s is the slope of the straight-line portions of the small-angle X-ray dispersion curves; D is the value of the fractal dimension; R_g is the radius of the rotation of the fractal aggregate; and $d_s = 2.58R_g$.

Impedance spectroscopy was carried out in the frequency range from 1 Hz to 5 MHz using a 1260 frequency response analyzer and a 1296 dielectric interface from Solartron. The measurements were performed in the temperature range from 300 to 950 K under dry air in a two-probe cell (DataLine). It has been checked that the electrochemical system remains linear up to 250 mV (rms) even at high temperatures; therefore, the applied alternating current voltage chosen was 100 mV (rms). Sputtered Pt was used as the electrodes. The samples for measurements had the following dimensions: diameter ≈ 0.7 cm and thickness ≈ 0.1 cm.

Electronic conductivity has been carried out following the procedure used by Lübke and Wiemhöfer.[15] A Pt microelectrode (contact radius of 120 μm ± 20 μm) was used as the blocking electrode for oxygen ions and pressed against the sample. A glass sealing (Heraeus, type IP 041) was applied onto the surface of the pellet around the tip of the microelectrode to encapsulate it and to prevent the oxygen exchange from the gas phase. The blocking character of the microelectrode has been checked thoroughly as described in the text. On the opposite side of the pellet, a two-phase mixture of Cu_2O/CuO, was used as the reversible electrode. The pellet was prepared from reagent-quality materials in the molar ratio 1/2. The steady-state current−voltage measurements were performed in the temperature range from 920 to 1020 K under dry N_2 atmosphere. The applied voltage (U) ranged from − 880 mV to + 380 mV in a stepwise change of 10 mV. A delay time of 200 to 300 s was applied to the cell before recording the steady-state current (I). The delay time was determined by recording the current versus time curve at a given temperature.

Results and Discussion

Investigation of Fractal Structure of the Dried Air SPH and CPH Samples. The density of the samples obtained by the SPH method was significantly higher than that of the samples obtained by the CPH method. This may be attributed to the self-organization of the precursor particles, which confirms the results of small-angle X-ray scattering obtained on sample III, which are presented in Table 1 (these results are analyzed in detail in ref 7). Because the fractal structure of samples I and II did not differ very much from the fractal structure of sample III, we present only results for sample III. As evidenced from Table 1, dried air SPH and CPH precipitates of sample III were characterized by three levels of fractal structures. They differ only in the type and size of fractals after transition from the second to the third dimensional level (Table 1); otherwise, they are quite similar.

(15) Lübke, S.; Wiemhöfer, H. D. *Solid State Ionics* **1999**, *117*, 229.

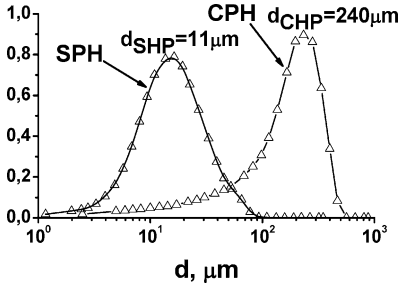

Figure 1. Size distribution of aggregating particles of samples SPH and CPH after annealing at $T = 870$ K.

At the third level, the SPH sample is typically made of mass-fractal (M), whereas CPH sample is made of surface-fractal agglomerates (S). SPH sample is mainly characterized by aggregation of unit fractal elements in the bulk, and the CPH sample is characterized by aggregation of unit elements on the surface. SPH and CPH samples, after drying in air and calcination, differ essentially in the strength of the aggregates (agglomerates), which was determined by a standard method as the maximum force at which the granules, as elastic-brittle solids, are crushed between two hard rests.[16] The size distribution curves for the aggregating particles of SPH and CPH samples, after heat treatment at 870 K, confirm this fact. Figure 1 shows that SPH and CPH samples have average conglomerate sizes of $d = 11$ μm and $d = 240$ μm, respectively. SPH conglomerates, with weaker bonds between particles, are easily crashed by ultrasound to smaller size.

In conclusion, the sequential precipitation of hydroxide (SPH method) allows the synthesis of stabilized ZrO_2 powders with easily breakable "soft" mass-fractal agglomerates that leads to the preparation of nanocrystalline ceramics. The presence of these breakable "soft" agglomerates favors the sintering process and decreases the sintering temperature of the ceramics. Table 2 shows clearly that a decrease of 200 K of the sintering temperature is observed on our sample prepared by the SPH method (sample n*o*. 8) if compared to the same composition sample obtained by solid-state reaction (sample n*o*. 5). Owing to the advantages of the SPH method, the conductivity was investigated only for these samples.

Structural and Electrophysical Properties of the Ceramic Samples. XRPD data showed that in ceramic samples I and II, cubic and tetragonal phases were present (Figure 2a). In sample I, the concentration of the tetragonal phase was higher than in sample II (Figure 2a and Table 3). Ceramic sample III is cubic single-phase (Figure 2a). Obviously, the phase composition depends on the chemical composition, namely, on the ratio of the stabilizing oxides CeO_2/Y_2O_3, and on their total amount. The smaller this ratio CeO_2/Y_2O_3 and the higher their sum, the higher the concentration of cubic phase in the ceramic. This clearly reveals the more effective influence of Y_2O_3 stabilizer.

Figure 3 shows the microstructure of samples I (a), II (b), and III (c). One can observe from this figure that the grain size of the ceramic samples I and II is approximately 250−300 nm, whereas the grain size of the sample III is approximately 2700−3000 nm. This significant difference of grain size may be due to a difference in the phase composition of samples I, II, and III because it is known that the coexistence of cubic and tetragonal phases inhibits grain growth.[17]

Figure 4 presents typical impedance diagrams for sample III, plotted in the Nyquist plane, and recorded at different temperatures (550, 575, 600, and 625 K), under dry air. The diagrams display two well-separated semicircles and a straight line, at low frequency. The high-frequency semicircle is attributed without doubt to the motion of the charged species into the grains of the ceramic ($C \approx 10^{-11}$ F), and the medium frequency one is attributed to their motion into the grain boundaries ($C \approx 10^{-7}$ F). Finally, the spike at low frequency is related to the polarization of the electrodes. As expected, the frequency of the maximum of the imaginary impedance increases as temperature increases, meaning that the charged species motion is thermally activated.

To analyze the impedance data, an electrical equivalent circuit made of series *RC* elements have been used. However, to take into account the fact that the semicircles are not centered on the real axis, we used a constant phase element (CPE) instead of pure capacitance *C*, as shown in the inset of Figure 4. Two serial (*R*//CPE) elements are necessary to fit the impedance diagrams, one being related to the bulk (b) and the other one to the grain boundary (gb) of the material. The electrode polarization at low frequency can be modelised by a CPE_{elect}. Finally, inductance (*L*) is used to take into account the contribution of the electrical wires, and their resistance which is very small (less than 1 Ω) has been ignored. Such a simple model perfectly applies for the three ceramics and in the whole temperature range investigated, from room temperature (RT) to 950 K. From the values of R_b and R_{gb}, the bulk conductivity, grain boundary conductance, and total conductivity of the ceramics have been determined.

Figure 5 shows the plots of the bulk conductivity (a) and the total conductivity (grain + grain boundary; b) as a function of the inverse of temperature for samples I, II, and III. Only a slight increase of the bulk conductivity can be observed with the increase of Y_2O_3 content in the ceramic, as shown in Table 4. Furthermore, the total conductivity is only slightly smaller than the bulk conductivity meaning that the resistances of the grain and of the grain boundary are of the same order of magnitude in the temperature range investigated. Around 900 K, the contribution of the bulk resistance to the total resistance (around 80%) is much greater than the grain boundary one, meaning that the grain boundary does not decrease the total conductivity to much extent compared to the intrinsic properties of the material, which is given by the bulk conductivity. This is an important advantage of the compounds of this solid solution added to

(16) Dubok, V.; Kabanova, M.; Pavlenko, N. *Powder Metall.* **1988**, *12*, 18.
(17) Karavayev, J. N.; Neuyimin, A. D.; Pankratov, A. A. *Inorg. Mater.* **1999**, *35*, (12), 1482.
(18) Xianshuang, X.; Zhe, Lu.; Xiqiang, H.; Xueqing, S.; Yaohui, Zh.; Wenhui, S. *Mater. Res. Bull.* **2006**, *41*, 1319.
(19) Naito, H.; Sakai, N.; Otake, T.; Yugami, H.; Yokokawa, H. *Solid State Ionics* **2000**, *135*, 669−673.
(20) Leonov, A. I.; Kostikov, Yu. P.; Ivanov, I. K.; Andreeva, N. S.; Trusova, E. M. *Inorg. Mater.* **1980**, *16* (9), 1576.

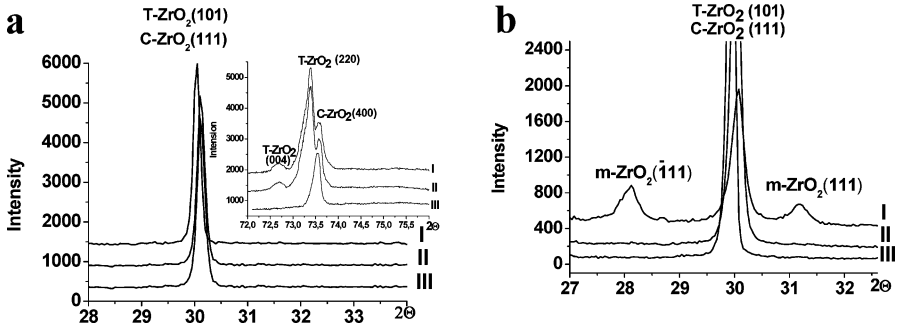

Figure 2. XRPD profiles of samples I, II, and III after sintering (a) and after measurements of conductivity up to 925 K (b).

Table 2. Literature Data Concerning the Characteristics of the Samples

no.	composition	σ_{total}, S/cm	$T_{measurement}$, K	$T_{sintering}$, K	method of synthesis	reference
1	0.84/0.16 ZrO_2-CeO_2	10^{-5}	950	1870	solid-state reaction	1
2	0.63/0.27/0.1 $ZrO_2-CeO_2-Y_2O_3$	10^{-3}	973	1953	solid-state reaction	19
3	0.098/0.882/0.02 $ZrO_2-CeO_2-Y_2O_3$	10^{-3}	1070	1570	precipitation from solution	2
4	0.63/0.27/0.1 $ZrO_2-CeO_2-Y_2O_3$	10^{-1}	1473	2023	solid-state reaction	13
5	0.828/0.092/0.08 $ZrO_2-CeO_2-Y_2O_3$	10^{-2}	1120	1870	solid-state reaction	9
6	0.88/0.12 $ZrO_2-Y_2O_3$	10^{-2}	1120	1720	hydrothermal method	18
7	0.893/0.057/0.05 $ZrO_2-CeO_2-Y_2O_3$	10^{-3}	970	1770	solid-state reaction	10
8	0.84/0.08/0.08 $ZrO_2-CeO_2-Y_2O_3$	10^{-3}	925	1670	precipitation from solution	our sample

Table 3. Some Characteristic of Samples I, II, and III[a]

sample no.	composition	ρ_{exptl}, g/cm^3	ρ_{theor}, g/m^3	C_t, mol %	Cc, mol %	V, Å^3
I	0.93/0.06/0.01 $ZrO_2-CeO_2-Y_2O_3$	5.846	5.82	0.82	0.18	68.12
II	0.88/0.09/0.03 $ZrO_2-CeO_2-Y_2O_3$	5.901	5.85	0.72	0.28	68.41
III	0.84/0.08/0.08 $ZrO_2-CeO_2-Y_2O_3$	5.66	5.80	0	1	134.26

[a] C_t refers to the concentration of the tetragonal phase, and Cc to concentration of cubic phase.

the fact that the presence of CeO_2 favors the sintering of the ceramics.

The activation energy of the conduction mechanism, according to the Arrhenius law

$$\sigma = \frac{\sigma_0}{T}\exp\left(-\frac{E_a}{RT}\right) \quad (1)$$

is shown in Table 4. The activation energy ranges from 0.97 to 1.04 eV which agrees well with an O^{2-} ion migration.

In Figure 5 it can be observed that sample I displays a hysteresis behavior at high temperature: the bulk conductivity suddenly decreases around 1 order of magnitude at this temperature. Such a behavior can be ascribed to the metastable character of this particular compound of the solid solution. Furthermore, conductivity measurements, performed on the same sample after keeping it for 3 months in air at RT, showed that the conductivity has strongly decreased. This behavior has been observed only on sample I. This metastable character has been confirmed by XRPD experiments performed on the sintered pellet after synthesis and after conductivity measurements. Figure 2b shows that a monoclinic phase appears in the oxide suggesting that the transformation from tetragonal to monoclinic occurs rapidly at high temperature on this particular sample. Indeed, the same XRPD experiments performed on samples II and III did not indicate any phase transformation, as shown in Figure 2b.

Table 4. Electrophysical Parameters of Samples I, II, and III at $T = 925$ K

sample no.	composition	E_a (eV)	σ_{bulk} (S cm^{-1})	σ_{total} (S cm^{-1})
I	0.93/0.06/0.01 $ZrO_2-CeO_2-Y_2O_3$	1.04	4×10^{-4}	2×10^{-4}
II	0.88/0.09/0.03 $ZrO_2-CeO_2-Y_2O_3$	1.04	2.2×10^{-3}	1.8×10^{-3}
III	0.84/0.08/0.08 $ZrO_2-CeO_2-Y_2O_3$	0.97	2.5×10^{-3}	2.4×10^{-3}

A comparison between the total conductivity of our herein studied compounds with the available data found in the literature, on the same or very close systems, shows that the conductivity of our ceramics is of the same order of magnitude as those reported in the literature (Figure 6 and Table 2), with the exception of compositions 0.84/0.16 ZrO_2-CeO_2[1] and 0.88/0.12 $ZrO_2-Y_2O_3$.[18]

According to the metastable character of sample I, electronic conductivity has been carried out on samples II and III only. The electronic conductivity was measured as a function of oxygen activity in the range from $a_{O_2} \approx 10^1$ to $a_{O_2} \approx 10^{-20}$ by using the Hebb−Wagner polarization technique with blocking Pt microelectrode. The oxygen activity is referred to a gas with $P_{O_2} = 1.013$ bar as the standard state. The goodness of the current−voltage curves is based on the assumption that the oxygen ion current is totally blocked at the encapsulated Pt microcontacts. Any leakage of oxygen through the glass sealing would lead to a partial non-blocking character of the Pt electrode and therefore to an increase of the recorded steady-state current. This point has been thoroughly checked before collecting data either by electrochemical techniques or by measuring steady-state current under dry N_2 and under dry air (20% O_2) at 750 °C. The $I-U$ curves are perfectly similar

(21) Leonov, A. I; Kostikov, Yu. P.; Ivanov, I. K; Andreeva, N. S; Trusova, E. M. *Inorg. Mater.* **1980**, *16* (No. 9), 1576.
(22) Naito, H.; Sakai, N.; Otake, T.; Yugami, H.; Yokokawa, H. *Solid State Ionics* **2000**, *135*, 669−673.
(23) Xianshuang, X.; Zhe, Lu.; Xiqiang, H.; Xueqing, S.; Yaohui, Zh.; Wenhui, S. *Mater. Res. Bull.* **2006**, *41*, 1319.

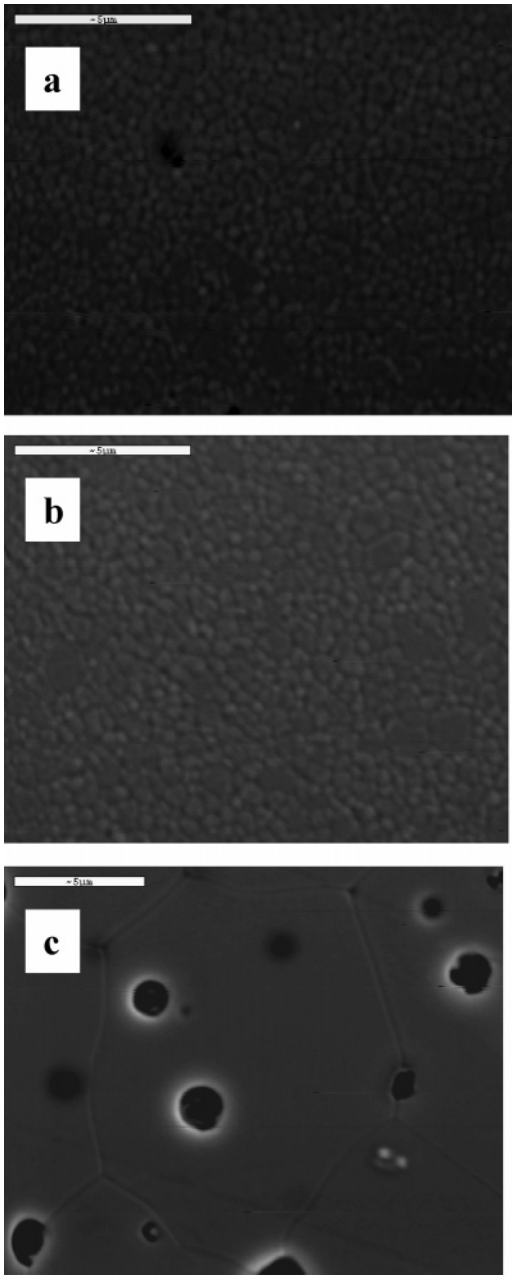

Figure 3. Microstructure of ceramic samples I (a), II (b), and III (c).

particularly in the high oxygen activity (a_{O_2}) domain, indicating that the microelectrode is a perfect ion blocking electrode. From the experimental $I-U$ curves, electronic conductivity can be calculated according to the following equation

$$\sigma_e(a_{O_2}) = \frac{1}{2\pi r}\frac{dI}{dU} \quad (2)$$

where r refers to the radius of the Pt electrode that we assume to be spherical.

Figure 7 shows the result of the electronic conductivity at different temperatures, that is, 920 K, 970 K, 995 K, and 1020 K, obtained on sample III (a pure cubic phase showing the highest conductivity). The curves show that the electronic conductivity remains very low ($\approx 10^{-5}$ S cm^{-1}) for a wide range of oxygen activity whatever the temperature.

It is known that electrical properties of a solid solution based on zirconium oxide with cerium oxide addition depend

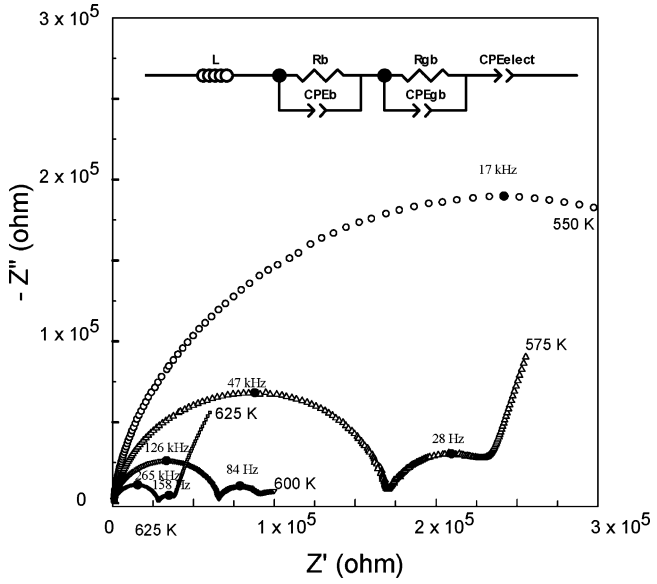

Figure 4. Impedance spectra for sample III at different temperatures (550 K, 575 K, 600 K, and 625 K). Electrical model used for the fitting of the experimental data.

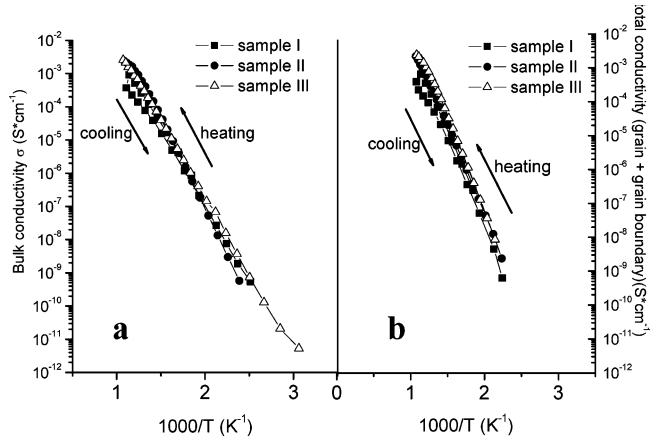

Figure 5. Temperature dependences of bulk conductivity (a) and total conductivity (grain + grain boundary; b) for samples I, II, and III.

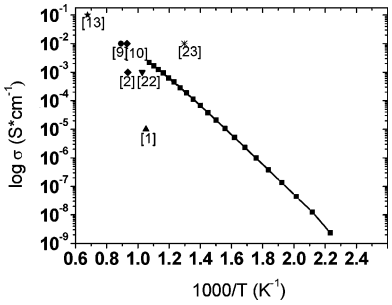

Figure 6. Temperature dependence of the total conductivity for sample III studied herein (black squares) and for some literature data (the reference number is shown in brackets).

appreciably on oxygen partial pressure. When a semiconducting metal oxide is put under reducing conditions (low oxygen activity for example), oxygen substoichiometry may occur owing to the chemical crystal−gas equilibrium. Therefore, at low oxygen activity the following equilibrium is shifted to the right with formation of oxygen vacancies and electrons (using Kröger−Vink notation for the defects):

$$O_O^X \leftrightarrow V_O^{\bullet\bullet} + 2e' + (1/2)O_2 \quad (3)$$

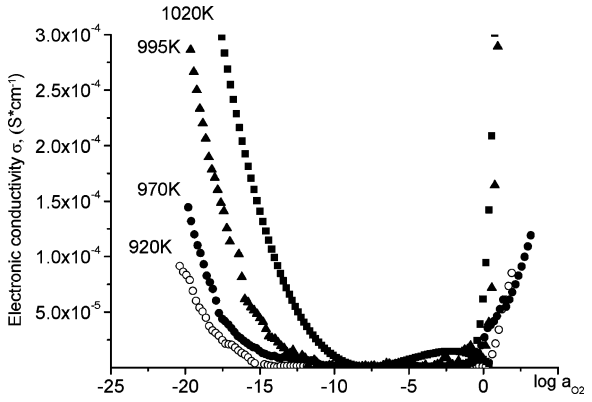

Figure 7. Oxygen partial pressure dependence of the electronic conductivity of sample III at different temperatures (920 K, 970 K, 995 K, and 1020 K).

The electrons are transferred to the Ce^{4+} ions that consequently are reduced to Ce^{3+} creating a mixed valence situation that leads to the appearance of n-type electronic conductivity

$$Ce_{Zr}^{X} + e' \leftrightarrow Ce'_{Zr} \quad (4)$$

For low a_{O_2} ($<10^{-10}-10^{-15}$ depending on the temperature) the n-type electronic conductivity increases. For high a_{O_2} (greater than 1), the electronic conductivity increases again because of increasing p-type conductivity. p-Type conductivity can be ascribed to the presence of oxygen vacancies due to the dopant Y_2O_3 and to the presence of some impurity that can be oxidized under high oxygen activity. The equilibrium (eq 3) is then shifted to the left with consumption of electrons or production of holes in the semiconductor. The equilibrium can also be written as

$$(1/2)O_2 + V_O^{\bullet\bullet} \leftrightarrow O_O^X + 2h^{\bullet} \quad (5)$$

The same experiments performed on sample II (72 mol % of tetragonal phase, small grains) showed the same behavior of the electronic conductivity with the appearance of the n-type electronic conductivity at even lower oxygen pressure. At 1020 K the n-type electronic conductivity appears at $a_{O_2} \approx 10^{-16}$ for sample II instead of 10^{-10} for sample III.

At 1020 K, an electronic conductivity $\sigma_e = 10^{-5}$ S cm^{-1} has been found at $P_{O_2} = 0.2$ bar (in air) for sample III. At this temperature, the total conductivity of this sample, $\sigma_t \approx 2.5 \times 10^{-3}$ S cm^{-1}, has been determined previously by impedance spectroscopy. Therefore, the electronic transference number is 0.4%. For sample II a slightly smaller electronic conductivity has been found at the same temperature and oxygen activity, that is, $\sigma_e = 6 \times 10^{-6}$ S cm^{-1} leading to a smaller electronic transference number of 0.3% ($\sigma_t = 2.2 \times 10^{-3}$ S cm^{-1}). As expected, these electronic transference numbers decrease as temperature decreases to reach values smaller than 0.1% at 920 K. These results indicate that these compounds are oxygen ion conductors even at high temperature.

For practical applications, oxygen ionic conductors must have electronic conductivity lower than 1%. Therefore, for these ceramics it is possible to determine the a_{O_2} range that can be used without exceeding this electronic conductivity. At 1020 K, for sample III, electronic conductivity will remain lower than 1% for $10^{-11} < a_{O_2} < 1$, and for sample II the domain increases to $10^{-17} < a_{O_2} < 1$. At 920 K, this range becomes $10^{-17} < a_{O_2} < 10$ for sample III and $10^{-19} < a_{O_2} < 10^2$ for sample II.

It had been concluded, from previous studies, that cubic structure favors a high value of the oxygen conductivity in comparison with tetragonal structure. On the basis of the above obtained results, it follows that the addition of CeO_2 to $ZrO_2-Y_2O_3$ compounds does not decrease considerably the bulk conductivity and offers some advantages on the properties of these ceramics even if it favors the formation of a tetragonal phase. The addition of CeO_2 to $ZrO_2-Y_2O_3$ compounds leads to a chemically stable phase when this amount does not exceed a certain value, for example, when the ratio Ce/Y < 6. Furthermore, it does not decrease the total conductivity of these compounds by improving the sintering procedure. It confirms the assumption, which was made by Leonov et al. some years ago,[20] that anionic conductivity of a solid solution based on zirconium oxide may be due to interactions of microdomains that have cubic and tetragonal structures. As the ratio CeO_2/Y_2O_3 increases from 1 to 3 (for samples III and II, respectively), the oxygen partial pressure domain, where electronic conductivity remains negligible, increases several orders of magnitude, particularly in the low pressure domain. This is also an important positive feature for practical applications.

Conclusion

It has been shown that sequential precipitation of hydroxides of the system $ZrO_2-Y_2O_3-CeO_2$ allows preparing precursors with mass-fractal organization, which are characterized by weak bounds between particles that determine their sintering activity.

It has been determined that phase composition, electrophysical properties, and stability of the structure of stabilized zirconium oxide $Y-Ce-ZrO_2$ are determined by its chemical composition, namely, the ratio of the stabilizing oxides CeO_2/Y_2O_3 and their total amount.

Ceramics containing CeO_2 can be synthesized at a low sintering temperature (1670 K). They are chemically stable. Despite the presence of the tetragonal phase, which inhibits the grain growth during sintering, they have a high value of bulk and total conductivity ($\sigma \approx 2 \times 10^{-3}$ S·cm^{-1} at $T =$ 925 K) and a low value of electronic conductivity (0.3−0.4% of total conductivity in air, $P_{O_2} = 0.2$ bar). The electronic conductivity does not exceed 1% in a wide range of oxygen partial pressures (for example, at $T = 920$ K, $10^{-17} < a_{O_2} < 10$ for sample III and $10^{-19} < a_{O_2} < 10^2$ for sample II).

Acknowledgment. O. Bohnke would like to thank Prof. H.-D. Wiemhöfer, from the Insitute of Inorganic Chemistry University of Münster (Germany), for helpful discussions on electronic conductivity equipment and measurements.

CM070319J